The evolution of information transmission in mammalian brain networks

Alessandra Griffa[1,2,3], Mathieu Mach[2], Julien Dedelley[2], Daniel Gutierrez-Barragan[4], Alessandro Gozzi[4], Gilles Allali[3,5], Joanes Grandjean[6,7], Dimitri Van De Ville[2,1], Enrico Amico[2,1]

[1] Department of Radiology and Medical Informatics, University of Geneva, Geneva, Switzerland

[2] Institute of Bioengineering, Center for Neuroprosthetics, École Polytechnique Fédérale De Lausanne (EPFL), Geneva, Switzerland

[3] Leenaards Memory Centre, Lausanne University Hospital and University of Lausanne, Lausanne, Switzerland

[4] Functional Neuroimaging Laboratory, Center for Neuroscience and Cognitive systems, Istituto Italiano di Tecnologia, Rovereto, Italy

[5] Division of Cognitive and Motor Aging, Department of Neurology, Albert Einstein College of Medicine, Yeshiva University, Bronx, NY, USA

[6] Department of Medical Imaging, Radboud University Medical Center, 6525 GA Nijmegen, The Netherlands

[7] Donders Institute for Brain, Cognition and Behaviour, Radboud University Medical Center, 6525 EN Nijmegen, The Netherlands

Corresponding authors

Alessandra Griffa - orcid.org/0000-0003-1923-1653
B1 0 265.042 (Campus Biotech Bâtiment B1)
Ch. des Mines 9
CH-1202 Genève
alessandra.griffa@gmail.com

Enrico Amico - orcid.org/0000-0001-6705-9689
H4 3 153.079 (Campus Biotech Bâtiment H4)
Ch. des Mines 9
CH-1202 Genève
enrico.amico@epfl.ch

Abstract

Brain communication, defined as information transmission through white-matter connections, is at the foundation of the brain's computational capacities that virtually subtend all aspects of behavior: from sensory perception shared across mammalian species, to complex cognitive functions in humans. How did communication strategies in macroscale brain networks adapted across evolution to accomplish increasingly complex functions? By applying a novel approach to measure information transmission in mouse, macaque and human brains, we found an evolutionary gradient from selective information processing, where brain regions share information through single polysynaptic pathways, to parallel information processing, where regions communicate through multiple parallel pathways. In humans, parallel processing acts as a major connector between unimodal and transmodal systems. Communication strategies are unique to individuals across different mammalian species, pointing at the individual-level specificity of information routing architecture. Our work provides compelling evidence that different communication strategies are tied to the evolutionary complexity of mammalian brain networks.

Introduction

Understanding how brain function can be supported by patterns of neural signaling through its structural backbone is one of the enduring challenges of network and cognitive neuroscience[1]. The brain is effectively a complex system, a network of neural units interacting at multiple spatial and temporal scales through the white-matter wiring[2,3]. *Information transmission through structural connections*, which can be defined as *brain communication*[1], give rise to macroscale patterns of synchronous activity–or functional connectivity–between remote areas of the brain. Communication processes are at the foundation of the brain's computational capacities that virtually subtend all aspects of behavior, from sensory perception and motor functions shared across mammalian species, to complex human functions including higher-level cognition[4]. From an evolutionary perspective, high communication efficiency at minimal structural wiring cost has long been recognized as a fundamental attribute constraining the evolution of neural systems[5–7]. Yet, quantitative and comparative assessments of macroscale communication processes in brain networks of increasing evolutionary complexity are lacking[1,8].

Systems-level neuroscience has made different attempts to map brain communication as interrelated patterns of macroscale structural and functional brain connectivity, highlighting strikingly complex structure-function interdependencies[9]. Structurally connected region pairs tend to have stronger functional connectivity than disconnected pairs[10,11], suggesting the presence of monosynaptic interactions[12]. Nonetheless, direct structural connections alone are not able to explain most of the dynamic functional repertoire observed in a functioning brain[13]. Beyond monosynaptic interactions, functional connectivity between remote brain areas is likely to emerge from more complex, higher-order communication mechanisms that involve larger groups of neural elements and their structural interconnections, by polysynaptic (multi-step) routing of neural information[1,14,15]. Higher-order communication in neural systems is important from both neurocognitive and evolutionary perspectives. Functional connectivity patterns extending beyond pairwise-connected regions (i.e., not constrained by the direct structural connections underneath) are highly specific to individuals, reflect behavioral traits[16], and have been identified across different mammals[17]. Moreover, functional patterns untethered from structure are dominant in cortical areas that underwent larger evolutionary expansion across primates, suggesting a relation between local information transmission mechanisms and evolution[18–20].

Nonetheless, the information transmission mechanisms implemented in mammalian brain networks are, to date, largely unknown. A first hypothesis has been that shortest structural

paths are favored for neural communication as they allow more direct (faster, metabolically less expensive) information transmission. In support of this hypothesis, brain networks of several mammalian and simpler species have short structural path length[21,22] at the price of a relatively high wiring cost[5]. This suggests that shortest paths contribute to efficient communication in brain networks and have been selected throughout evolution despite their high wiring cost. However, relying on path length as the sole measure of information routing may be an oversimplification[14]. Shortest-path communication explains a limited portion of functional connectivity[10] and excludes a large fraction of brain network connections and near-optimal alternative pathways from the communication process[23]. Recent studies have started to account for more complex mechanisms of information routing, such as parallel communication (i.e., relay of information through multiple, parallel communication pathways)[23–26] or convergent routing (i.e., neural signals' interaction through convergent pathways)[27,28]. Indeed, in many real-world systems, information transmission unfolds through numerous alternative pathways[29]. Nevertheless, we do not know what is the relative contribution of single-pathway versus parallel-pathway communication in mammalian neural systems.

Comparative neuroimaging provides instruments to understand the emergence of function across evolution[21,30]. Evidence of similarities between neural systems in different species are assumed to reflect common organizational principles and functions that may be evolutionarily preserved. In contrast, regions showing the greatest changes between humans and other species highlight neural changes that may account for features of cognition unique to humans. It has been shown that the overall topology of the structural and functional brain networks is preserved across evolution[21,22] despite large variations in brain size and cortical expansion[20]. However, differences in local connectivity patterns and functional dynamics exist[31–33]. Recent reports suggest that mammalian neural processing is organized along multiple hierarchies from unimodal to transmodal regions, describing how information from distinct neural populations are integrated and segregated across the cortex[20,34]. Yet, a comprehensive account of how evolution has shaped cortical organization requires a way to measure how brain communication mechanisms change *in vivo* across species, while also taking into account the underlying structural architecture. Are macroscale brain communication mechanisms preserved across mammalian species? Or contrarily, are there distinct brain communication strategies relating to mammals' evolution? , In particular, was there a shift from selective (single-pathway) to parallel processing across evolution to support increasingly complex brain functions? These questions do not have trivial answers and demand for new ways of assessing brain communication across different species.

Here we apply a novel approach, rooted in information theory, to measure polysynaptic information transmission in macroscale brain networks. Taking advantage of structural and functional connectivity information extracted from multimodal brain data (i.e., functional MRI, diffusion MRI, tract tracing), we explore the intricate pathways of communication in the mouse, monkey and human connectomes. We employ information-theoretical principles[24,35,36] to identify the structural pathways selected for neural communication by different neural systems, and measure the level of selective and parallel information processing across the different species. We report a strong evolutionary gradient in the brain communication dynamics of mammals, with predominant selective information routing in lower mammalian species such as mice and macaques, morphing into more complex communication patterns in human brains. Parallel communication strategies appear to have acted as a major connector of unimodal (sensory, attentional) and transmodal (fronto-parietal, default mode) areas in the human brain, possibly contributing to the evolution of more complex cognitive functions in humans. Notably, we also found that brain communication strategies are highly specific to individuals across the different mammalian species. Our results link for the first time the complexity of macroscale brain communication dynamics inferred from *in vivo* data to an evolutionary gradient across mammalian lineages. These findings pave the way to a deeper understanding of how brain communication and its relationship to function have evolved across species.

Results

We propose a new framework to identify communication pathways in brain networks and investigate their evolution in three mammalian species of increasing phylogenetic complexity: mice, monkeys, and humans (Fig. 1). These species represent distinct mammalian lineages and include animal models (mice, monkeys) often used in translational research. We aimed to formally test two general assumptions on brain communication dynamics. First, due to the noisy nature of neural signaling, neural messages transmitted through the structural brain network can keep at most the same amount of information present at the source region[24,35]. This holds true for many communication systems where the information content tends to decay as one moves away from the information source[25]. Second, in an information transmission process, messages are typically *relayed* through a set of statistically independent steps[44]; i.e., neural messages do not contain memory of the transmission process itself and communication happens in a Markovian fashion[37]. These two assumptions –information decay and memoryless transmission– are formally summarized by a fundamental principle of information theory, the data processing inequality (*DPI*)[36], which we here apply to cross-species structural data and fMRI recordings (Online Methods). Given a structural network representing the white matter wiring of the brain, we first identify sets of short polysynaptic paths connecting each pair of brain regions (Fig. 1a). Next, we quantitatively assess which and how many of those structural paths are effectively selected for neural communication. To this aim, we quantify fMRI-derived mutual information measures along the paths (Fig. 1b) to assess the *DPI* on those paths (Fig. 1c). From here, a parallel communication score can be computed for every pair of brain regions, by counting the number of paths that respect the *DPI* (Fig. 1d). Parallel communication scores portray a spectrum of communication strategies from *selective information processing*, where brain regions selectively exchange information through a single pathway, to *parallel information processing*, where regions communicate through multiple, parallel pathways (Fig. 1e). We assessed parallel communication scores at the individual and group levels, and summarized them for distinct brain systems and single brain regions in comparison to appropriate null models. Finally, we compared the distribution of selective and parallel information processing across the three different mammalian species.

Data for this study consisted of open-source whole-brain structural connectivity matrices and individual resting-state functional MRI recordings of 100 healthy human subjects, 9 macaque monkeys, and 10 wild-type mice, all in their young adulthood (Online Methods, Supplementary Table 1; see below for replication datasets). Group-representative structural connectivity matrices with comparable number of brain regions were derived from diffusion MRI and tract tracing data, and weighted by the Euclidean distance between connected

regions (Supplementary Figure 1). Individual-level mutual information matrices were computed from fMRI recordings of comparable duration and temporal resolution across species.

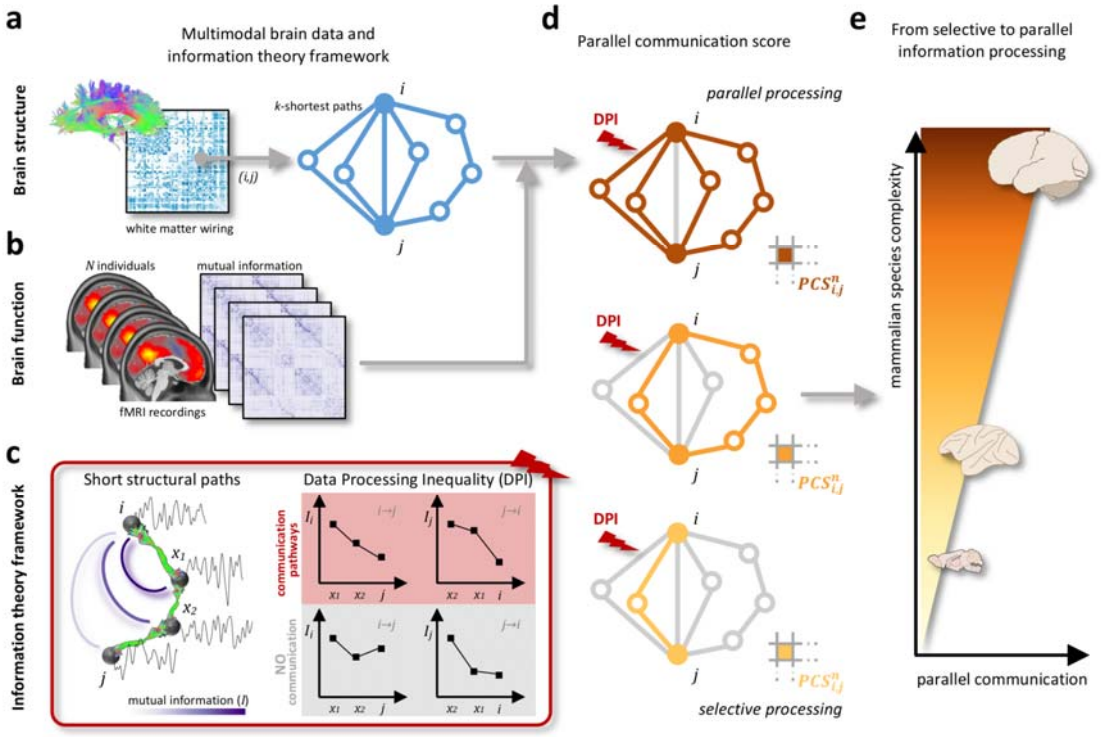

Figure 1 Identifying communication pathways in macroscale brain networks. (a) A weighted and symmetric structural connectivity matrix summarizes the white matter wiring of the brain for each species. For every pair of brain regions *(i, j)*, the 5 shortest structural paths (light blue) connecting the two regions are identified using the *k*-Shortest path algorithm[23]. **(b)** For every subject (human participant or animal), the mutual information between region pairs is computed from *z*-scored regional timecourses obtained from fMRI recordings. **(c)** By analyzing the mutual information values along each structural path, the data processing inequality (*DPI*) is used to assess whether the specific paths represent valid communication channels between regions *i* and *j*. Left panel: two brain regions *i, j* are connected by a structural path crossing regions x_1, x_2; green lines represent direct structural connections (white matter fibers). Each region is associated with a neural activity-related timecourse; the amount of information shared by two regions is quantified by their mutual information *I* (darker and thicker arcs indicate stronger *I*). Right panel: a structural path (i, x_1, x_2, j) is labeled as communication (relay) channel if the pairwise mutual information values do not increase along the (undirected) path (first row, red shading); it is not a communication channel otherwise (second row, gray shading: $I_{j,i} > I_{x2,i}$). **(d)** A parallel communication score (*PCS*) is computed at the individual level (i.e., for every subject *n*) and for every pair of brain regions *i, j* by counting the number of structural paths that serve as relay channels between the two regions. **(e)** Parallel communication scores are investigated across mammalian species, highlighting a spectrum of communication strategies from selective information

processing (light yellow; low *PCS*), to parallel information processing (dark brown; high *PCS*).

Parallel communication in brain networks follows an evolutionary gradient across mammalian species

Using our approach we found that, in mammalian brains, polysynaptic structural paths are used to relay information in a 'Markovian'-specific, sequential processing fashion. For all the three considered species, the whole-brain density of relay communication pathways (i.e., the percentage of structural paths respecting the *DPI*) was higher than in a strict null model preserving the structural connectivity architecture and the multivariate statistics of fMRI timecourses (Online Methods; $p < 10^{-5}$ for all species). This held true when considering either the first shortest path connecting region pairs (mean±standard deviation across individuals: humans = 39.5±3.8%; macaques = 37.1±6.0%; mice = 37.1±2.3%), or longer paths (humans = 33.0±5.6%; macaques = 29.5±5.7%; mice = 28.2±5.9%), showing that relay communication is not limited to the shortest path only (Fig. 2a). Specifically, the communication density level of the shortest and second shortest paths was comparable for all the three species, but decayed right after. Next, we assessed the amount of parallel communication between all brain region pairs. We found that, on average, the parallel communication score (*PCS*) progressively increases from mice and macaques to humans (median [5-, 95-percentile] across region pairs: mice = 1.30 [0.20, 2.50]; macaques = 1.33 [0.11, 2.56]; humans = 1.52 [0.11, 3.02];). This is particularly evident when considering the long-tailed distribution of human brain network communication as compared to the animals (Fig. 2b). The three species' *PCS* distributions were pairwise statistically different (two-sample Kolmogorov-Smirnov tests human-macaque: $D_{4950,3321} = 0.157$, $p < 10^{-42}$; human-mouse: $D_{4950,3003} = 0.171$, $p < 10^{-47}$; macaque-mouse: $D_{3321,3003} = 0.058$, $p < 10^{-4}$). These results indicate that, as brain complexity increases across the phylogenetics tree, interareal communication is increasingly subserved by parallel processing (Fig. 2).

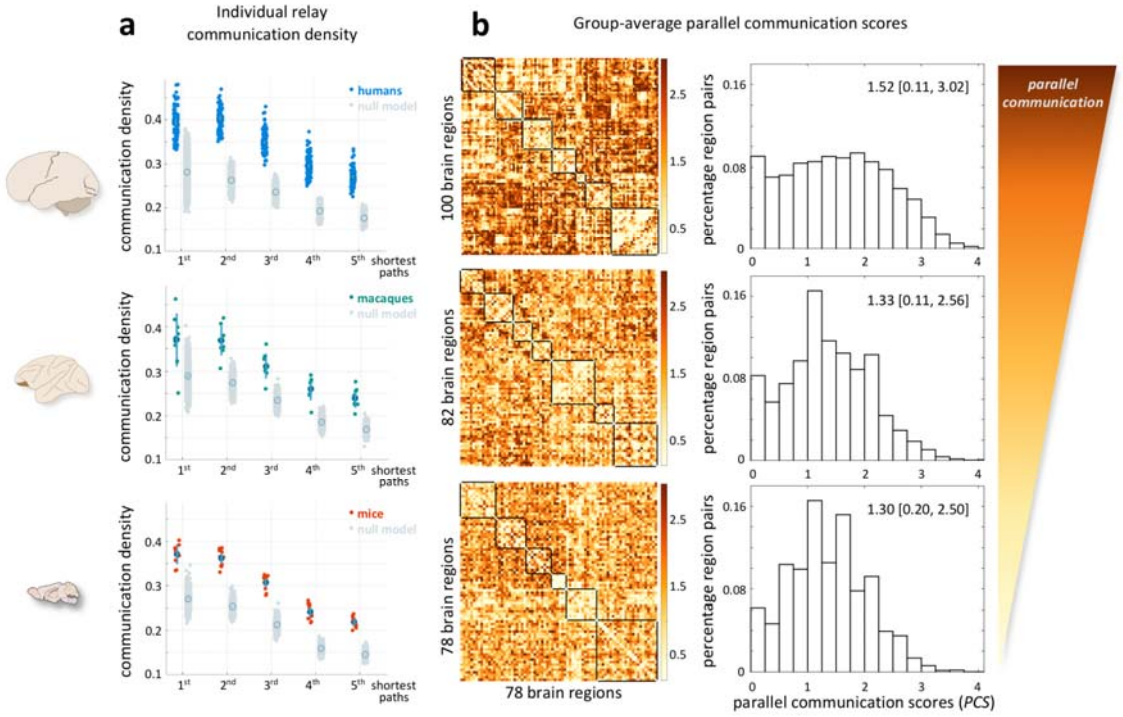

Figure 2 Parallel communication follows an evolutionary gradient across mammalian species. Left: drawing of human, macaque, and mouse brains; each row in the figure corresponds to one species. **(a)** Box plots representing the percentage of short paths in individual brain networks used for relayed communication (i.e., respecting the *DPI*). Each colored dot represents an individual; gray dots represent species-specific null distributions obtained from permutation of mutual information values (Online Methods); circles and vertical bars indicate mean ± one standard deviation across individuals or randomizations. Paths are grouped according to the 1st up to the 5th shortest path between region pairs, showing that relay communication is not limited to the 1st shortest path only. **(b)** Group-average parallel communication score (*PCS*) matrices representing *PCS*s between every pair of brain regions, averaged across individuals. For each species, brain regions are organized according to meaningful functional circuits which are highlighted by black squares along the matrices' diagonals (Online Methods). On the right, the histograms of the average *PCS* scores across region pairs highlight an evolutionary gradient from mice, with lower *PCS*s and mainly selective information processing, to humans, with higher *PCS*s and presence of parallel communication. Median [5-, 95-percentile] *PCS* values for each species are reported atop each histogram.

Communication complexity is species-dependent and relates to the functional organization of mammalian brains

When evaluating the spatial localization of the relay communication pathways, we found that it followed the characteristics of each species' functional cortical architecture (Fig. 3). Specifically, in lower species the relay (mostly sequential) pathways mainly encompassed

unimodal/multimodal regions spanning the barrel, auditory and somatomotor cortices in mice, and the visual, somatomotor and dorsal attention cortices in macaques (Fig. 3a). In humans we found similar evidence of relay sequential processing in unimodal and multimodal areas, but also a high concentration of parallel communication pathways in *transmodal regions* including association cortices of the executive-control network and the precuneus of the default mode network (Fig. 3a; note the different color scales across species).

Next, we investigated the communication patterns at the level of region pairs within and between different brain functional systems (Online Methods, Supplementary Fig. 3, 4). In mice, the relay pathways mainly connected brain nodes belonging to unimodal systems, including auditory, barrel, somatomotor and visual cortices (Fig. 3b). A similar distribution was observed for relay pathways in macaque networks, mainly connecting visual with somatomotor and dorsal attentional regions. However, a gradient transitioning towards transmodal regions started to appear between the default mode network and attentional systems (Fig. 3b). In humans, stronger (parallel) relay communication mainly connected somatosensory and attention regions with executive-control and default mode systems, forming *cross-modal parallel streams* between unimodal and transmodal regions (outside-diagonal entries in Fig. 3b). Notably, these patterns were stable at the individual level. We report in Fig. 3c the amount of relay communication (average *PCS*s) within unimodal systems, within transmodal systems, and between unimodal and transmodal systems for each subject. Within species, the amount of relay communication varied between systems, with transmodal networks consistently presenting the lower amount of relay communication (Kruskal-Wallis tests, $p < .05$) (Fig. 3c). Across species, relay communication within unimodal systems decreased with increasing phylogenetic complexity (mice > macaques > humans, $H(2) = 22.45$, $p = .000013$), while cross-modal communication between unimodal and transmodal regions strongly increased (mice < macaques < humans, $H(2) = 46.44$, $p < 10^{-10}$), with humans presenting 30% larger *PCS*s than macaques (Supplementary Fig. 2). Relay communication within transmodal systems was relatively stable across species ($H(2) = 6.24$, $p = .044$). Taken together, these findings show that communication strategies are highly heterogeneous across the brain network and are partially preserved across evolution. However, phylogenetically older species demonstrate more developed relay communication for lower-order processing between unimodal and multimodal regions. Conversely, the human brain is characterized by stronger parallel communication that serves as the main neural processing stream between unimodal and transmodal areas[34,38].

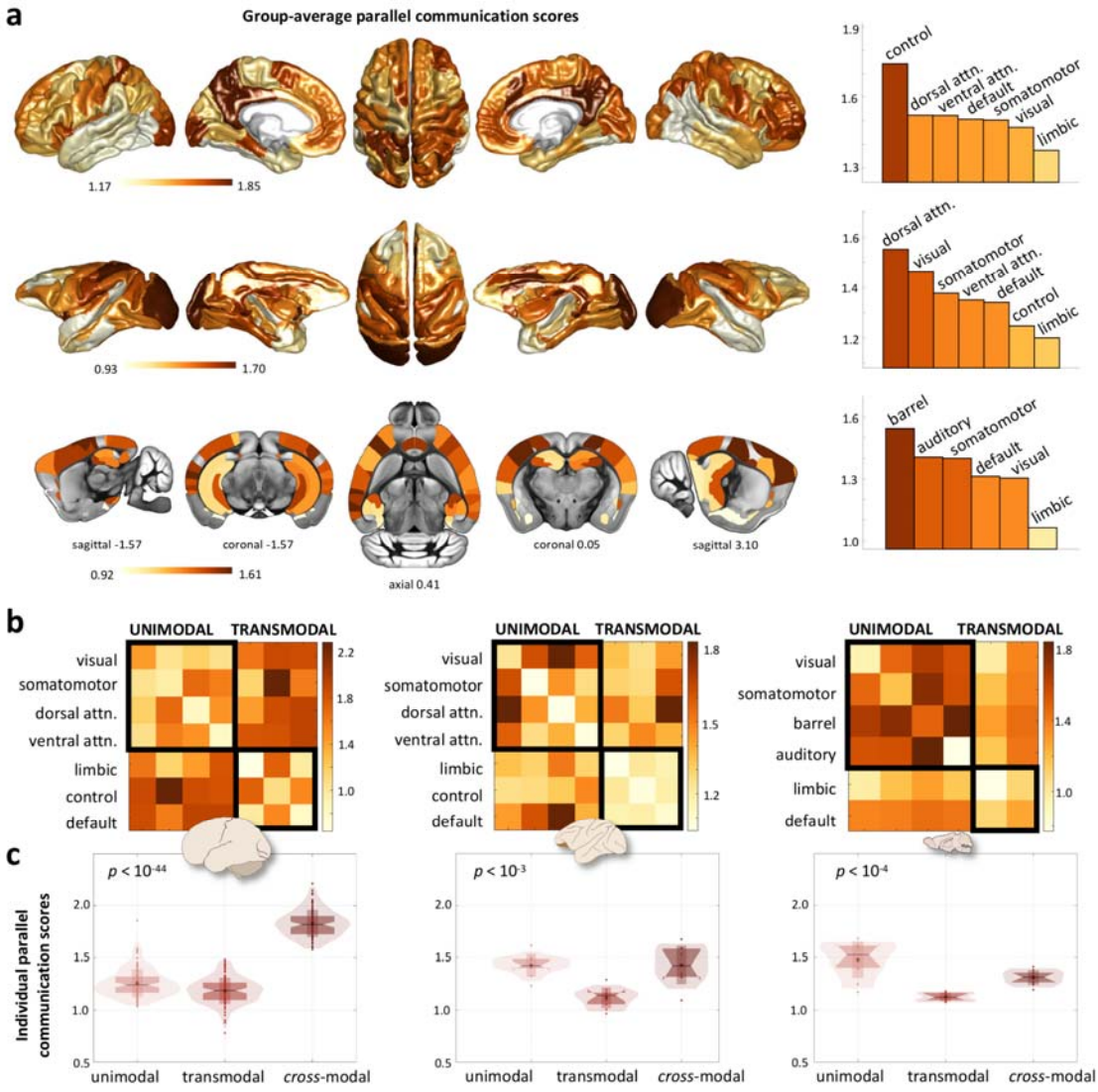

Figure 3 Relay communication strategies reflect the functional organization of mammalian brains. (a) Cortical distributions of relay communication, quantified as the average *PCS* of each brain region with the rest of the brain network (first row: human, *fsaverage6* cortical surface; second row: macaque, *F99 template*; third row: mouse, *ABI template*). For each species, the light yellow-to-brown colormap is scaled between the 5th and 95th percentiles of the cortical values. On the right, the average nodal communication scores per brain system are represented in the bar plots. **(b)** Average *PCS*s within and between brain systems, for humans, macaques and mice. Brain systems have been organized into unimodal/multimodal regions (upper-left black square) and transmodal regions (lower-right black square). **(c)** Average *PCS*s between unimodal systems, between transmodal systems, and between unimodal and transmodal systems (*cross*-modal communication) for individual subjects. In the box plots, each dot represents an individual; vertical bars indicate mean ± standard deviation; notch bars indicate median and 1st-3rd quartiles; shaded areas indicate 1st-99th percentiles. Kruskal Wallis *p*-values for within-species comparisons are reported. Control = executive-control; Dorsal attn. = dorsal attention; ventral attn. = ventral attention.

316

317 **Relay communication patterns are unique to individuals**

318

319 Our results revealed a link between relay information processing strategies and phylogenetic
320 complexity in the mammalian brain. Are the observed communication patterns specific to
321 individual subjects within single species? We addressed this question by exploring the
322 identifiability properties[39,40] of the parallel communication matrices reported in Fig. 2, across
323 the three different species. To this aim, the fMRI recording of each subject was split into two
324 sections of equal duration. From these, test and retest parallel communication matrices were
325 computed. Note that, at the individual level, the matrices' entries (*PCS*s) can take integer
326 values between 0 and 5, with 0 indicating no relay communication, 1 indicating perfectly
327 selective information processing, and 5 strongly parallel information processing. We
328 quantified the similarity between test and retest data as the percentage of brain regions'
329 pairs with exactly the same *PCS* (Jaccard similarity index). The individual identifiability
330 through relay communication patterns was then quantified as the success rate (SR), i.e., the
331 percentage of subjects whose identity was correctly predicted out of the total number of
332 subjects for each species[40]. We found that parallel communication scores allow to identify
333 individual mammals in all the three species, at a level that exceeds chance-level (humans:
334 SR = 87.0%, null = 0.9±1.0%; macaques: SR = 66.7%, null = 11.2±10.3%; mice: SR =
335 60.0%, null = 10.6±9.2%) (Fig. 4a,b). However, individual identifiability decreased from
336 humans, to macaque, to mice. Intriguingly, the major contribution to individual identifiability
337 was given by brain regions pairs that, on average, tends to communicate through multiple
338 parallel rather than selective pathways. When splitting region pairs into two groups ('*low-*
339 *PCS*', '*high-PCS*') according to group-average parallel communication scores, the success
340 rate obtained from *high-PCS* values was higher than the one obtained from *low-PCS* values
341 for both humans and macaques (*PCS* threshold = 1.3; humans: $SR_{low\text{-}PCS}$ = 73.0%, $SR_{high\text{-}PCS}$
342 = 85.0%; macaques: $SR_{low\text{-}PCS}$ = 44.4%, $SR_{high\text{-}PCS}$ = 55.5%; mice: $SR_{low\text{-}PCS}$ = 40.0%, $SR_{high\text{-}}$
343 $_{PCS}$ = 40.0%; see Supplementary Table 2 for alternative thresholds) (Fig. 4c,d). No
344 differences were found in mice. Taken together, these data suggest that, within the inherent
345 constraints of each species, individual subjects may implement distinct communication
346 strategies to relay neural information through the brain network, particularly when
347 considering higher-order communication mechanisms such as parallel communication.

348

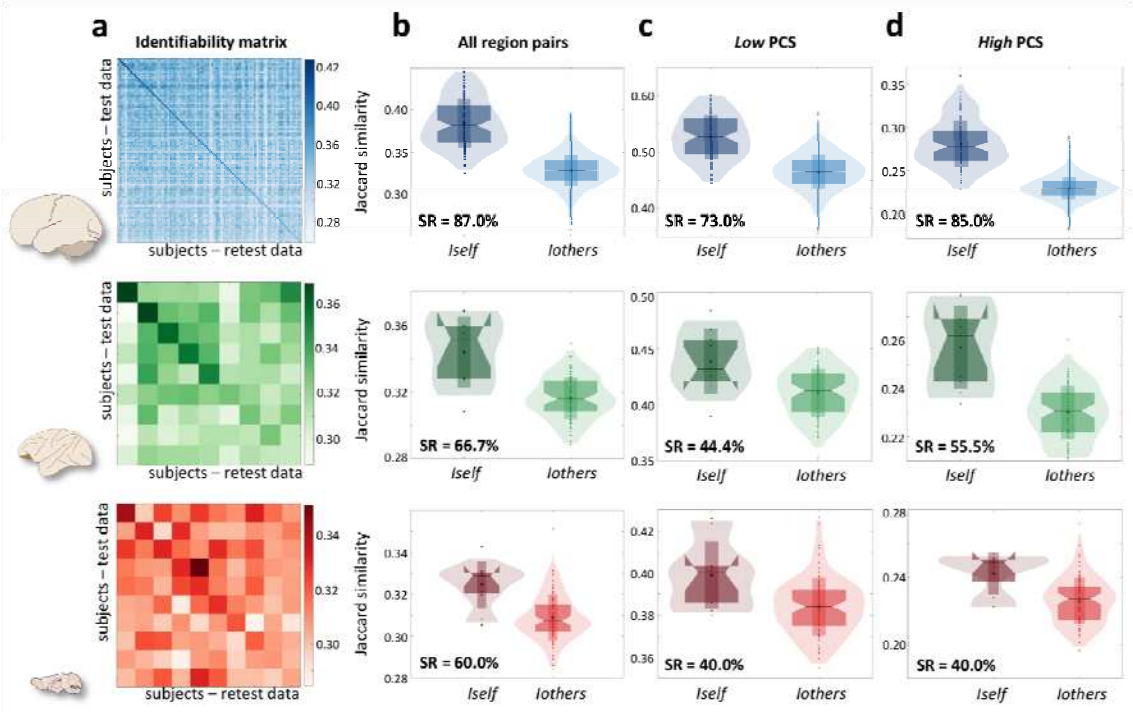

Figure 4 Parallel communication is unique to individuals. Left: drawing of human, macaque, and mouse brains; each row in the figure corresponds to one species. **(a)** Identifiability matrices for the three species, reporting subjects' similarities between test (rows) and retest (columns) parallel communication data. Test-retest similarity was quantified with the Jaccard similarity index. **(b)** Box plots representing *self*-similarity (*Iself*, diagonal entries of the identifiability matrix) and *others*-similarity (*Iothers*, out-diagonal entries of the identifiability matrix) values. **(c)** *Self*- and *others*-similarity values when considering only region pairs with *low* parallel communication scores (PCS ≤ 1.3 on average). **(d)** *Self*- and *others*-similarity values when considering only region pairs with *high* parallel communication scores (PCS > 1.3 on average). The success rate (SR) for subjects' identification is reported for each pair of box plots. In the box plots, vertical bars indicate mean ± standard deviation; notch bars indicate median and 1st-3rd quartiles; shaded areas indicate 1st-99th percentiles.

Robustness, sensitivity and replication analyses

To ensure the validity of our results, we asked whether parallel communication scores and their cross-species gradients could be explained by the different structural connectome architectures and multivariate statistical properties of fMRI recordings alone. To this aim, we constructed null distributions of parallel communication scores for each species, by randomly shuffling the fMRI time series across brain regions and computing surrogate *PCS*s on the original structural connectome architecture (n = 3000) (Online Methods, Supplementary Fig. 5). By z-scoring the real *PCS* scores with respect to the null distributions and applying

appropriate statistical thresholds, we show that our findings do not trivially derive from structural connectivity and fMRI statistical properties alone. In particular, the gradient of increasing parallel communication from mice to humans (Fig. 2, Supplementary Fig. 6, 7, 8) and the cortical topographies of parallel communication density across species (Fig. 3, Supplementary Fig. 9) remained significantly different from the null ones.

Next, we investigated whether results were sensitive to some methodological choices, including number of brain regions (brain parcellation), fMRI time series length, and number of subjects. We found that our results are robust to these factors. In humans, *PCS* scores and their cortical topographies were comparable when subdividing the cortex into 100 or 200 regions of interest (Supplementary Fig. 10, 11). However, we observed lower *PCS* scores when using a finer-grain parcellation with 400 regions (Supplementary Fig. 10). This is expected since brain connectivity and structure-function relationship have been shown to vary with the number of brain regions[41]. *PCS* scores tended to increase for longer fMRI time series, but this effect did not impact inter-species differences nor *PCS* cortical topographies (Supplementary Fig. 10, 11), and it could relate to the improved reliability of functional connectivity estimation for longer scan lengths[42]. Whenever possible, data from the three species were matched both in the number of brain regions and fMRI scan duration. The effect of the number of subjects on *PCS* scores was minor (Supplementary Fig. 12).

Finally, we assessed the replicability of our findings by analyzing a total of six distinct datasets (Online Methods). We found that parallel communication scores (Fig. 2, Supplementary Fig. 12), their cortical topographies (Fig. 3, Supplementary Fig. 11, 13, 14), and the gradient of parallel communication between unimodal and transmodal regions across species (Fig. 3, Supplementary Fig. 15) were consistent when considering alternative datasets. In particular, overall cortical topographies were unaltered when considering awake or anesthetized macaques and mice (Supplementary Fig. 13, 14). However, awake animals tended to have larger parallel communication between transmodal regions and between transmodal and unimodal regions (*cross-modal* streams), but unchanged communication between unimodal regions as compared to anesthetized animals (Supplementary Fig. 16). These state-dependent differences were smaller than the ones observed between mice and macaques, and humans. The amount of parallel communication in awake macaques and mice was lower than the amount observed in humans, confirming the parallel communication gradient along the evolutionary axis.

Discussion

How networked neural elements intercommunicate at the systems level, ultimately giving rise to brain function, stands as one of the most intriguing and unsolved questions of modern neurosciences. *In vivo* measurements of brain structure and activity are providing us with windows of opportunities for modeling communication in brain networks, across different animal species. We propose here to bring a piece to this puzzle, by investigating the link between communication strategies in large-scale brain networks, on the one side, and the evolutionary complexity of mammals' brain functions, on the other.

By introducing a novel approach to formally test and detect relay communication pathways in brain networks, we provide compelling evidence that this link exists, and that different communication strategies are tied to the evolutionary complexity of mammalian brain networks along two main organizational principles. The first principle is the increasing recruitment of parallel communication pathways, which evolves from predominantly selective information processing mechanisms in mice, to parallel information processing in humans. The second principle involves the development of cross-system communication through parallel pathways that connect together functionally specialized brain regions (i.e., somatomotor, visual) with transmodal ones (i.e., fronto-parietal, default mode).

Specialized, unimodal brain systems are organized as serial, hierarchical streams where raw sensory information is relayed through stepwise progressive circuits to guide attention and direct actions[20,34]. Consistent with this hierarchical polarity, we found that unimodal regions are mainly characterized by selective information processing through single pathways, as quantified by low parallel communication scores. This held true for all the investigated mammalian species, suggesting that unimodal selective information processing is phylogenetically preserved. On the other hand, transmodal regions present a more complex and less understood organization. Back in 1998, Mesulam hypothesized that "the flow of information for intermediary [transmodal] processing displays patterns consistent with parallel and re-entrant processing"[34]. Our findings consolidate this view by showing–in a data-driven and hypothesis-independent way–that information transmission between unimodal and transmodal regions evolved from selective to parallel streams across species with increasing cognitive abilities. Parallel communication could therefore represent a more complex form of information transmission beyond hierarchical processing, which might support integration of perceptual modalities into more complex textures of cognition.

What evolutionary mechanisms may have promoted a higher involvement of parallel communication strategies in humans? According to the tethering hypothesis proposed by Buckner and Krienen[20], the fast cortical expansion of transmodal regions in humans compared to non-human primates has led to the untethering of these regions from developmental anchor points. This process allowed human transmodal regions to develop unique cytoarchitectonic[43] and connectional[31] fingerprints, unbound from the hierarchical architecture of topographically distant unimodal systems[38]. The same process may have also favored the development of new information transmission strategies (parallel communication) to bridge hierarchical unimodal and distributed transmodal regions. Indeed, in humans we observed the largest parallel communication scores in regions that underwent the largest cortical expansion across evolution, including fronto-parietal association cortices and precuneus[44]. In addition, parallel information transmission may be functional to specific processing needs of unimodal-transmodal communication supporting cognition. Recent computational studies suggest that brain regions with largest allometric scaling privilege fidelity rather than compression of incoming signals from unimodal areas[24]. High-fidelity information transmission may be achieved through parallel streaming of redundant signals, expression of a more resilient communication process.

Our results show that parallel communication also contributes to the individual specificity of communication strategies in brain networks. Selective and parallel information transmission patterns allowed identifying subjects in a group with significant accuracy, across different mammalian species. This indicates that the individual layout of relay communication pathways constitutes an important fingerprint of brain organization, and that this fingerprint is present even at lower phylogenetic levels (i.e., in mice). Brain regions that tend to communicate through parallel rather than selective streams, including transmodal regions, provided the largest contribution to subject identifiability. Consistently, fMRI activity of association and default mode cortices displays larger inter-individual variability in human and nonhuman primates compared to lower-order regions[40,45,46]. The role of transmodal cortices in individual identifiability is consistent with their protracted neurodevelopment and function in higher-order cognition, and it could partially explain the identifiability gradient observed from humans to macaques, to mice, with mice displaying lower parallel communication levels and lower identifiability. However, the identifiability gradients may also be explained by a larger homogeneity among laboratory animals compared to human samples in terms of genetic pedigree and environmental conditions.

Importantly, the evolutionary gradient from selective to parallel information processing and the cortical topographies of parallel communication patterns were not explained by cross-

479 species differences of structural connectivity architecture, statistical properties of fMRI data,
480 or conscious (i.e., awake *vs* anesthetized) state. In keeping with previous studies[22], we
481 found that the overall distribution of short structural path lengths was similar between
482 species, with comparable amounts of 2-step, 3-step, and 4-step pathways. Relative cross-
483 species differences of parallel communication were unchanged when contrasting data with
484 respect to a strict, species-specific null model which preserves multivariate fMRI statistics.
485 When considering fMRI data from awake and anesthetized animals, we found similar cortical
486 distributions of parallel communication patterns, with unimodal regions dominated by
487 selective information processing. This finding is in line with the observation that resting state
488 networks are globally preserved in conscious and unconscious states[17,47]. However, we
489 found that the overall amount of communication tends to increase during wakefulness,
490 particularly when considering information transmission streams interconnecting transmodal
491 regions with the rest of the brain network. A shift of the communication regime toward more
492 abundant and (partially) parallelized polysynaptic information transmission may
493 mechanistically support functional integration, inter-network cross-talk, and rich functional
494 repertoires departing from the underlying monosynaptic connectivity constraints, which have
495 been repeatedly observed in awake primates and mice compared to the anesthetized
496 ones[17,47,48].
497
498 Several higher-order communication models have been proposed to explain integration of
499 information between multiple brain network elements[1]. Nonetheless, the exact polysynaptic
500 communication mechanisms underlying macroscale neural signaling remain unclear.
501 Intriguingly, brain communication models mostly rely on the assumption of memoryless
502 (Markovian) information transmission[49]. This hypothesis is pervasive in network
503 neuroscience[37] but has never been formally tested in the brain. Our work adds to the field in
504 two important ways. First, it introduces a new approach to extract relay communication
505 pathways from multimodal brain data, in a way that is agnostic to specific communication
506 models and grounded in fundamental information-theoretic principles. Secondly, it formally
507 probes the existence of memoryless information transmission in brain networks by
508 introducing an empirical way to assess deviations from Markovity through the data
509 processing inequality[35]. Our results show that Markovian communication is present in brain
510 networks across different mammalian species, is not limited to the shortest structural path,
511 but involves multiple and less optimal structural paths in a way that is species-dependent
512 and consistent with the evolutionary complexity of each investigated species.
513
514 Polysynaptic memoryless information transmission is a simple form of higher-order
515 communication. There is no reason to assume that macroscale neural communication is

limited to such a particular form. Brain network hierarchies may confer neural signals a memory of the regions previously visited along a path, thus modifying neural communication pathways in a context-dependent manner[49]. This process would result in non-Markovian communication regimes. The brain may also implement complex multi-object interactions not attributable to information transmission alone, such as synergistic or modulatory behaviors between multiple brain regions[37,50]. Biologically, these communication strategies may shape important features of the mammalian brain, such as cortical temporal hierarchies[51,52] or receptive time windows for attentional processes[53]. This work only focuses on Markovian information transmission and does not inform us about other complementary information processing strategies. As such, absence of relay communication (i.e., violation of the data processing inequality) may indicate absence of any communication between those particular brain regions, or communication through more complex information encoding mechanisms. Notwithstanding the evidence that selective and parallel Markovian pathways serve as important information streams for multimodal integration between unimodal and transmodal systems[34,38], we speculate that low parallel communication scores between transmodal regions may indicate predominance of more complex communication regimes in these areas. In addition, sensory input decoding within the highly clustered unimodal systems (diagonal entries of the parallel communication matrices, Fig. 3b) may be supported by synergistic processes within dense structural motifs[54]. How these macroscale communication mechanisms may have adapted to changing environments over the evolution of mammalian brains remains an exciting open field of research, to which the present work adds a first foundation.

Acknowledgements

We thank Prof. Joaquín Goñi, Prof. Dante Mantini and Prof. Martijn Van den Heuvel for their critical suggestions and helpful discussions; Dr. Kelly Shen for the help with the main macaque dataset; Dr. Maria Giulia Preti and Dr. Raphaël Liégeois for the processing of human data. Human data were provided by the Human Connectome Project, WU-Minn Consortium (Principal Investigators: David Van Essen and Kamil Ugurbil; 1U54MH091657) funded by the 16 NIH Institutes and Centers that support the NIH Blueprint for Neuroscience Research; and by the McDonnell Center for Systems Neuroscience at Washington University. A.Gr. acknowledges funding from the Swiss National Science Foundation (Grant No. 320030_173153). E.A. acknowledges financial support from the SNSF Ambizione project "Fingerprinting the brain: network science to extract features of cognition, behavior and dysfunction" (Grant No. PZ00P2_185716). A.Go. acknowledges funding from the European Research Council (ERC, #DISCONN; no. 802371), the Brain and Behavior

553 Foundation (NARSAD, 25861), the NIH (1R21MH116473-01A1) and the Telethon foundation
554 (GGP19177).

Online Methods

Human data

We used Magnetic Resonance Imaging (MRI) data of the Human Connectome Project (HCP), U100 dataset (HCP900 data release), which includes 100 unrelated healthy adults ('*h-HCP*' dataset, 64 males; mean age = 29.1 ± 3.7 years)[55]. Informed consent forms, including consent to share de-identified data, were collected for all subjects (within the HCP) and approved by the Washington University institutional review board. All methods were carried out in accordance with relevant guidelines and regulations. MRI scans were performed on a 3T Siemens Prisma scanner and included the following sequences: Structural MRI: 3D Magnetization Prepared Rapid Acquisition with Gradient Echoes (MPRAGE) T1-weighted, TR = 2400 ms, TE = 2.14 ms, TI = 1000 ms, flip angle = 8°, FOV = 224 × 224, voxel size = 0.7 mm isotropic. Diffusion-weighted MRI: spin-echo Echo-Planar Imaging (EPI), TR = 5520 ms, TE = 89.5 ms, flip angle = 78°, FOV = 208 × 180, 3 shells of b-value = 1000, 2000, 3000 s/mm^2 with 90 directions plus 6 b-value = 0 s/mm^2 acquisitions. One session of 15 min resting-state functional MRI (fMRI): gradient-echo EPI, TR = 720 ms, TE = 33.1 ms, flip angle = 52°, FOV = 208 × 180, voxel size = 2 mm isotropic, recorded with two phase-encoding directions (right-left and left-right). HCP minimally preprocessed data[56] were used for all acquisitions.

Group-level structural connectivity. A group-representative structural connectome between 100 cortical regions of interest (Schafer parcellation[57]) was obtained from the 100 unrelated HCP subjects. Different cortical parcellation resolutions were explored in supplementary analyses (200- and 400-region Schaefer parcellations[57]). Briefly, diffusion-weighted scans were analyzed using MRtrix3[58], including the following steps: multi-shell multi-tissue response function estimation; constrained spherical deconvolution; tractogram generation with 10^7 output streamlines. The Schaefer cortical atlas was used to parcellate the cortex into 100 (200, 400) regions and generate individual structural connectomes, from which a group-representative structural connectome was computed. The binary architecture of the group-representative connectome was obtained by including only the structural connections retrieved in 100% of the subjects. This step is meant to minimize the number of false positives in the group-representative network. The group-representative connectome was then weighted by the Euclidean distance (in millimeters) between region pairs' centroids (Supplementary Fig. 1a). This choice was motivated by the exigence of homogenizing structural connections' weights across species (see also *Mapping relay communication pathways in brain networks*).

Individual functional information. Resting-state fMRI data were pre-processed according to a state-of-the-art pipeline[18] including: general linear model regression of nuisance signals (removal of linear and quadratic trends; removal of motion regressors and their first derivatives; removal of white matter and cerebrospinal fluid signals and their first derivatives). 100 (200, 400) regional time series were obtained by averaging voxel-wise time series across all voxels belonging to each region of interest. The mutual information between region pairs was computed from the histograms of the z-scored time series, binned with a step of 0.5. This bin size was chosen by comparing real and null mutual information values, with null values obtained from multivariate gaussian data, and by assessing the fingerprinting accuracy[39] of mutual information across bin sizes (Supplementary Fig. 17). Only the first 800 time points (9.6 min) were considered for mutual information computation for consistency with other species data (Supplementary Table 1; other time series lengths were explored in supplementary analyses, Supplementary Fig. 10). Mutual information matrices obtained from left-right and right-left phase-encoding acquisitions were averaged to obtain a single 100x100 (200x200, 400x400) mutual information matrix per subject (Supplementary Fig. 1c).

Replication datasets. Analyses were repeated considering sub-samples of the whole U100 dataset (Supplementary Fig. 12).

Macaque data

We used structural and functional monkey data from TheVirtualBrain project[59]. The fMRI dataset included 9 adult male rhesus macaque monkeys (8 Macaca mulatta, 1 Macaca fascicularis) aged between 4 and 8 years ('*q-TVB*' dataset). All methods were carried out in accordance with relevant guidelines and regulations and have been previously described[59]. Briefly, animals were lightly anesthetized before their scanning session and anesthesia was maintained using 1-1.5% isoflurane. The scanning was performed on a 7T Siemens MAGNETOM head scanner included: Structural MRI: 3D MPRAGE T1-weighted sequence, 128 slices, voxel size = 0.5 mm isotropic. Diffusion-weighted MRI: EPI sequence, 24 slices, b-value = 1000 s/mm^2, 64 directions, recorded with two opposite phase-encoding directions. One session of 10 min resting-state functional MRI (fMRI): 2D multiband EPI sequence, TR = 1000 ms, 42 slices, 1 X 1 X 1.1 mm^3 voxel size.

Group-level structural connectivity. We used the whole-brain macaque structural connectome provided by TheVirtualBrain[59], which summarizes the brain connectivity between 82 regions of interest (Regional Map parcellation of Kötter and Wanke[60]) and

includes inter-hemispheric connections. Briefly, the structural connectome was obtained by optimizing tractography-derived structural connectivity matrices with respect to a reference tracer-derived connectivity matrix and averaging across animals[59]. For cross-species consistency reasons, we considered undirected structural connectivity information. That is, in the final structural connectome, two regions are connected if at least one unidirectional connection exists between the two regions. Structural connections were weighted by the Euclidean distance (in millimeters) between region pairs' centroids (Supplementary Fig. 1a).

Individual functional information. Resting-state fMRI data were pre-processed by others, as previously described[59]. Briefly, the processing pipeline included motion correction, high-pass filtering, regression of white matter and cerebrospinal fluid signals, spatial normalization and smoothing. Z-scored regional time series (Regional Map parcellation) including 600 time points (10 min) were used to compute individual mutual information matrices (bin size = 0.5, consistently with other species) (Supplementary Fig. 1c).

Replication dataset. Analyses were repeated on an independent dataset of 9 adult rhesus macaque monkeys (Macaca mulatta) aged between 5 and 12 years scanned on a vertical Bruker 4.7T primate dedicated scanner at Newcastle University[61] ('*q-NCS*' dataset). Raw data were publicly available through the Primate Data Exchange (PRIME-DE) initiative[62] and included the following MRI sequences: Structural MRI: Modified Driven Equilibrium Fourier Transform (MDEFT) T1-weighted, TR = 2000 ms, TE = 3.75 ms, TI = 750 ms, voxel size = 0.6 x 0.6 x 0.62 mm^3. Two runs of 10.8 min resting-state fMRI: TR = 2600 ms, TE = 17 ms, voxel size = 1.2 mm isotropic. All animals were scanned awake. MRI data preprocessing included: T1-weighted volumes denoising[63], skull-stripping (FSL[64]), N4 bias field correction, spatial normalization to the F99 template obtained from the SumDB database (http://brainvis.wustl.edu/sumsdb/public_archive_index.html), and registration to fMRI native space (ANTs[65]); fMRI volumes were coregistered (FSL[66]), corrected for nuisance signals including 6 motion signals, average white matter and cerebrospinal fluid signals, and band-pass filtered to the band 0.01-0.15 Hz. Z-scored regional time series (Regional Map parcellation) of the two concatenated fMRI runs were used to compute individual mutual information values (bin size = 0.5). The fMRI scans were concatenated to reach a number of time points comparable with the other datasets (500 time points, 21.6 min).

Mouse data

We used open-source fMRI data of 10 male wild-type mice aged 6 months ('*m-AD3*' dataset), available at https://openneuro.org/datasets/ds001890[67]. All methods were carried

out in accordance with relevant guidelines and regulations and have been previously described[17,68]. Briefly, animals were anesthetized with 4% isoflurane before their scanning session and maintained with 0.5% isoflurane and a 0.05 mg/kg/h medetomidine infusion[69]. The scanning was performed on a 11.75T Brucker BioSpin scanner and included: Structural MRI: spin-echo turboRARE sequence, TR = 2750 ms, TE = 30 ms, FOV = 17 x 11 mm^2, matrix dimension = 200 x 100 voxels, slice thickness = 0.35 mm. One session of 10 min resting-state functional MRI (fMRI): gradient-echo EPI sequence, TR = 1000 ms, TE = 15 ms, matrix dimension = 90 x 60 voxels.

Group-level structural connectivity. A mouse structural connectome between 78 cortical regions covering the isocortex, cortical subplate, and hippocampal formation, as defined in the Allen Brain Atlas, was derived from published viral tracing data[70]. In more details, the binary architecture of the structural connectome was assessed according to the following steps: (i) we considered the right-hemisphere ipsilateral and contralateral connections reported by Oh and colleagues[70]; (ii) we symmetrized the right-hemisphere ipsilateral connections (i.e., we considered a connection between ipsilateral regions *i* and *j* to be present if at least one of the two tracts (*i*→*j*), (*j*→*i*) was detected); (iii) we duplicated the symmetrized ipsilateral connections to the left hemisphere (in absence of more detailed information, we therefore assume equal intra-hemispheric connectivity in the right and left hemispheres); (iv) we transposed the contralateral connections of the right hemisphere to the left hemisphere; (v) to minimize false positives due to minor tissue segmentation artifacts, we excluded connections with connectivity strength < $10^{-3.5}$, as suggested in[70], where the connectivity strength was defined as the total volume of segmented pixels in the target normalized by the injection site volume. The binary structural connectome was then weighted by the Euclidean distance between region pairs' centroids obtained from the Allen Brain Atlas (CCF v3, © 2004 Allen Institute for Brain Science. Allen Mouse Brain Atlas. Available from: http://www.brain-map.org/) (Supplementary Figure 4).

Individual functional information. Resting-state fMRI data were pre-processed as previously described[68]. Briefly, the processing pipeline included motion correction, automatic brain masking, spatial smoothing (FWHM = 0.45 mm), high-pass filtering (0.01 Hz cut-off), and automated nuisance removal based on independent component analysis. Z-scored regional time series (78-region Allen Brain Atlas parcellation) including 600 time points (10 min) were used to compute individual mutual information matrices (bin size = 0.5) (Supplementary Fig. 1c).

Replication datasets. Analyses were repeated on two independent datasets. The first one included 51 male wild-type mice scanned at 3 months ('*m-CSD1*' dataset)[71]. MRI acquisitions were performed on a 9.4T Brucker BioSpin system on anesthetized animals (3.5% isoflurane, maintained with 0.5% isoflurane and a 0.05 mg/kg/h medetomidine infusion) and included a 6-min resting-state fMRI recording: gradient-echo EPI sequence, TR = 1000 ms, TE = 9.2 ms, flip angle = 90°, field of view = 20 x 17.5 mm^2, matrix size = 90 x 70 voxels, slice thickness = 0.5 mm. FMRI volumes were preprocessed using the same pipeline as the *m-AD3* dataset. The average time series of the 78 cortical regions (360 time points, 6 min) were z-scored and used to compute individual mutual information matrices (bin size = 0.5). Analyses were repeated considering sub-samples of the whole *m-CSD1* dataset (Supplementary Fig. 12).

The second dataset included 10 C57Bl6/J adult male mice ('*m-GG*' dataset, < 6 months old) subject to surgery for headposts placement, MRI habituation and awake fMRI acquisition, as previously described[17]. MRI acquisitions were performed at the IIT laboratory in Rovereto (Italy) on a Bruker Biospin 7T scanner and included a 32-min resting-state fMRI recording: single-shot EPI sequence, TR = 1000 ms, TE = 15 ms, flip angle = 60°, voxels size = 0.23 x 0.23 x 0.6 mm^3. fMRI preprocessing included exclusion of the first 2 min of recording, time series despiking, motion correction, nuisance signals regression (average cerebrospinal fluid and motion signals plus their temporal derivative and corresponding squared regressors), data censoring (Framewise Displacement > 0.075 mm), band-pass filtering (0.01-0.1 Hz), spatial smoothing (FWHM = 0.5 mm) and spatial normalization[17]. Average time series were computed for 66 regions of interest, which represents a subset of the 78 Allen Brain Atlas regions (data for bilateral regions CA1, CA2, CA3, dorsal and ventral endopiriform nucleus, and frontal pole were not available). The first 600 time points (10 min) were used for the computation of individual mutual information matrices (z-scored time series binning = 0.5).

Assignment of cortical regions to resting state networks

For the *human dataset*, each cortical region was assigned to one the seven resting state networks (RSNs) defined by Yeo and colleagues and according to the Schaefer parcellation [57,72]. For the *macaque dataset*, each cortical region was first associated with one or multiple Brodmann areas according to the CoCoMac Regional Map of the macaque cortex[60,73–75]. Each Brodmann area was then assigned to one of the seven RSNs defined by Yeo and colleagues[72] using a majority voting procedure and published atlases in MNI space[76]. Finally, Regional Map regions of the macaque cortex were assigned to Yeo RSNs with a similar majority voting procedure (Supplementary Fig. 3). For the *mouse dataset*, each cortical region was assigned to one out of 6 RSN as identified by Zerbi and colleagues using

independent component analysis of resting-state fMRI data[77]. The assignment was done through a majority voting procedure (Supplementary Fig. 4). Note that the default mode network (DMN) has been consistently identified in humans[78], macaques[79] and mice[80,81], suggesting a conservation of this network across mammalian species. In our mouse cortex subdivision[77], the DMN includes bilateral hippocampal regions (CA1, CA2, CA3 hippocampal fields, subiculum and dentate gyrus), and lateral (ectorhinal and temporal association areas) and prefrontal (infralimbic, prelimbic and perirhinal areas) isocortices, while it excludes other regions which have been reported by others, such as the retrosplenial cortex[82]. For all species, RSNs were assigned to unimodal or transmodal systems according to established cortical subdivisions[38].

Mapping information transmission pathways in brain networks

In this work we introduce a new approach to infer relay communication pathways from multimodal neuroimaging data. The approach builds upon and extends an information theoretical framework proposed in previous work[35], and aims at identifying polysynaptic (multi-step) structural pathways selected for information transmission in macroscale brain networks. Information theory is a branch of mathematics that studies the transmission of information through communication systems[36] and has found several applications in neuroscience[83,84]. It allows model-independent analysis of noisy data, such as the fMRI ones.

Structural brain network and structural paths. Let's consider a structural brain network as an undirected graph $G \equiv \{V, W\}$ formed by a set of N nodes $V = \{v_1, v_2, \ldots, v_N\}$ and a connectivity matrix $W = [w_{i,j}]$, with $w_{i,j} > 0$ distance between directly connected region pairs v_i , v_j and $w_{i,j} = \infty$ otherwise. In this work we assigned $w_{i,j}$ equal to the Euclidean distance (in millimeters) between the centroids of regions v_i , v_j. This choice has two motivations. First, the distance between region centroids can be easily computed across different datasets, thus allowing to select homogeneous structural connectivity weights across species. Second, this choice conceptually links information transmission in brain networks with the sender-channel-receiver schematics proposed in electronic communication by Shannon[35,85]. A path between a source node v_i and a target node v_j is a sequence of pairwise connected and non-repeating nodes $\Omega_{i,j} = \{v_i , v_a , v_b , \ldots , v_j\}$. The shortest path $\Omega_{i,j}^{SP}$ between regions v_i , v_j is the path of minimal length (i.e., minimal Euclidean distance, in the case of this work) connecting the two regions. The path length is computed as the sum of edge weights along the path. In this work we identified the first $k = 5$ k-shortest paths

$\Omega_{i,j}^{k-SP}$ connecting each region pair v_i , v_j[86]. K-shortest path ensembles identify meaningful trade-offs between efficiency and resiliency for putative communication processes in brain networks[23]. The choice of k was dictated by the fact that, for $k = 5$, all edges of the structural brain network participate in at least one k-shortest path[23].

Functional information along structural paths. Each node v_i is associated with a neural activity-related fMRI time series X^i that can be interpreted as the realization of a discrete random variable with probability mass function $p_i(x^i)$. The amount of shared information between two random variables can be quantified as their mutual information $I(X^i, X^j) = \sum_{x^i \in X^i} \sum_{x^j \in X^j} p_{i,j}(x^i, x^j) log_2(p_{i,j}(x^i, x^j)/p_i(x^i)p_j(x^j))$, with $p_{i,j}(x^i, x^j)$ joint probability distribution between X^i, X^j. The sequence of pairwise mutual information values along a structural path $\Omega_{i,j}$ with respect to the source node i is defined as $\Phi_{i,j} = \{I(X^i, X^a), I(X^i, X^b), \dots, I(X^i, X^j)\}$. We estimated the fMRI time series probability mass functions from the z-scored time series' histograms with appropriate binning. Different bin sizes between 0.05 and 2.00 were explored and evaluated with respect to (i) corresponding mutual information values for multivariate Gaussian processes $\aleph(0, I)$; (ii) individual identifiability scores[39]. We selected the smallest bin size for which (i) the mutual information values obtained from real data (*h-HCP* dataset) were larger than expected for a multivariate Gaussian process $\aleph(0, I)$, and (ii) the individual identifiability score reached a maximum plateau (Supplementary Fig. 17).

Data Processing Inequality (DPI). The *DPI*, a fundamental principle of information theory, states that the amount of information available at a target node j about a source node i cannot be increased through operations performed along the transmission path. Mathematically, the DPI states that if $X^i - X^a - X^j$ is a Markov chain, then $I(X^i, X^a) \geq I(X^i, X^j), I(X^a, X^j) \geq I(X^i, X^j)$, i.e., the mutual information does not increase along the chain[36]. Note that the double inequality condition derives from the fact that a Markov chain has no directionality information, i.e., if $X^i - X^a - X^j$ is a Markov chain, then $X^j - X^a - X^i$ is also a Markov chain. The *DPI* can be extended to Markov chains of any length. Conceptually, the *DPI* embeds two assumptions about the information transmission process: the first one is that (neural) messages transmitted through the structural infrastructure (brain network) can keep at most the same amount of information present at the source region (*information decay*). The second one is that (neural) messages do not contain memory of the transmission process itself and communication happens in a Markovian fashion (*memoryless transmission*).

Identification of information transmission pathways in brain networks. We used the DPI to test (deviation from) Markovian behavior. Each k-shortest structural path was labeled a relay communication pathway if the *DPI*s along the paths were satisfied. Note that here we use the wording *relay communication* in Shannon's sense. That is, we aim to characterize the presence of memoryless information transmission processes, with information decay along the path measured through mutual information values.

Parallel communication scores (PCSs). We define the parallel communication score $PCS_{i,j}^{n}$ between a pair of brain regions v_i , v_j as the number of k-shortest paths connecting the two regions which respect the *DPI*, with n indicating the subject. Note that, given the choice of $k = 5$, *PCS* scores can assume integer values between 0 and 5, and that $PCS_{i,j}^{n} = PCS_{j,i}^{n}$. A *PCS* score equal to 0 is interpreted as absence of (Markovian) information transmission between two regions; a *PCS* score equal to 1 is interpreted as presence of *selective information processing* through a single information transmission pathway; PCS scores larger than 1 are interpreted as presence of progressively increasing *parallel information processing* with information transmission through multiple parallel pathways (Fig. 1). *PCS* scores were computed for every pair of brain regions and every subject, for all investigated datasets. Parallel communication information was summarized at the group-level by computing a group-average parallel communication matrix PCS^{avg} for each dataset, and its corresponding histogram (Fig. 2). In addition, node-average, RSN-average, and system-average *PCS* scores were computed by averaging the parallel communication scores over the corresponding region pairs (Fig. 3).

Null model. A null model was defined by randomly shuffling the raw fMRI time series across brain regions while preserving the original structural connectivity information (Supplementary Fig. 5). Note that with this randomization we are preserving the statistical properties of both the original functional and structural data, since we are merely rearranging spatially fMRI time series across the brain network. Parallel communication matrices were then computed for each randomization following the above-described procedure. For each dataset, the randomization was repeated 3000 times *per* subject, which allowed to build 3000 group-average parallel communication matrices (Supplementary Fig. 6). Each region pair was therefore associated with a null distribution of group-average *PCS* values including 3000 elements. To assess whether group-average *PCS* scores observed in real data could be trivially explained by the structural connectivity architecture and the multivariate statistical properties of fMRI data, which are both preserved in the null model, we adopted two

strategies. The first one consisted of *PCS* scores screening by z-scoring individual group-average scores $PCS_{i,j}^{avg}$ with respect to the corresponding null distribution; z-scored where thresholded at 1.96 (Supplementary Fig. 7). The second strategy consisted of analyzing the *PCS* scores with false discovery rate (FDR)-corrected *p*-values < .05 (*FDR < .05*), with p-values computed as the number of entries in the null distribution exceeding the real *PCS* score (Supplementary Fig. 8).

Subject identifiability analysis

For each investigated dataset, fMRI time series were split into two parts of equal duration and considered as test and retest data. From these, test and retest parallel communication matrices were computed for each subject. An identifiability matrix summarizing test-retest subjects' similarities was then obtained for each dataset. Diagonal entries of the identifiability matrix represent subjects' *self*-similarity between test and retest data ('*Iself*'); outside-diagonal entries represent inter-subject similarity ('*Iothers*') (Fig. 4)[39]. The similarity between test and retest parallel communication matrices was assessed with the Jaccard index, defined as the size of the intersection divided by the size of the union of two label sets. For example, a Jaccard index equal to 0.3 indicates that 30% of brain region pairs have exactly the same *PCS* score, which can take integer values between 0 and 5. The level of individual identifiability was quantified with the success rate (SR) defined as the percentage of test subjects whose identity was correctly predicted out of the total set of retest subjects[40]. The subject identifiability analysis was repeated when considering only region pairs with, on average, low (high) *PCS* scores for the computation of test-retest similarities. Different thresholds defining low (high) *PCS* scores were explored (Supplementary Table 2).

Data and material availability

The data that support the findings of his study are available on the Human Connectome Project platform (db.humanconnectome.org) for human data; OpenNeuro[59], Zenodo[59], and INDI PRIMatE Data Exchange (fcon_1000.projects.nitrc.org/indi/indiPRIME.html) platforms for macaque data; OpenNeuro[67], XNAT[71], and Mendeley[17] platforms for mouse data. The derived brain matrices necessary to reproduce the main analyses of this study are available on Zenodo. The code (in MATLAB) and sample brain matrices are available as maintained version on A.Gr.'s GitHub repository (github.com/agriffa/BrainComm_mammalian_evolution).

879 **References**

880

881 1. Avena-Koenigsberger, A., Misic, B. & Sporns, O. Communication dynamics in complex
882 brain networks. *Nat Rev Neurosci* **19**, 17–33 (2018).
883 2. Bullmore, E. & Sporns, O. Complex brain networks: graph theoretical analysis of
884 structural and functional systems. *Nature Reviews Neuroscience* **10**, 186–198 (2009).
885 3. Bassett, D. S. & Sporns, O. Network neuroscience. *Nat Neurosci* **20**, 353–364 (2017).
886 4. Medaglia, J. D., Lynall, M.-E. & Bassett, D. S. Cognitive Network Neuroscience. *Journal
887 of Cognitive Neuroscience* **27**, 1471–1491 (2015).
888 5. Kaiser, M. & Hilgetag, C. C. Nonoptimal Component Placement, but Short Processing
889 Paths, due to Long-Distance Projections in Neural Systems. *PLOS Computational Biology*
890 **2**, e95 (2006).
891 6. Bullmore, E. & Sporns, O. The economy of brain network organization. *Nature Reviews
892 Neuroscience* **13**, 336–349 (2012).
893 7. Chen, Y., Wang, S., Hilgetag, C. C. & Zhou, C. Features of spatial and functional
894 segregation and integration of the primate connectome revealed by trade-off between
895 wiring cost and efficiency. *PLOS Computational Biology* **13**, e1005776 (2017).
896 8. Lynn, C. W. & Bassett, D. S. The physics of brain network structure, function and control.
897 *Nat Rev Phys* **1**, 318–332 (2019).
898 9. Mišić, B. *et al.* Network-Level Structure-Function Relationships in Human Neocortex.
899 *Cereb Cortex* **26**, 3285–3296 (2016).
900 10. Goñi, J. *et al.* Resting-brain functional connectivity predicted by analytic measures of
901 network communication. *PNAS* **111**, 833–838 (2014).
902 11. Hagmann, P. *et al.* Mapping the Structural Core of Human Cerebral Cortex. *PLOS
903 Biology* **6**, e159 (2008).
904 12. Singer, W. Neuronal Synchrony: A Versatile Code for the Definition of Relations?
905 *Neuron* **24**, 49–65 (1999).
906 13. Honey, C. J. *et al.* Predicting human resting-state functional connectivity from

907 structural connectivity. *PNAS* **106**, 2035–2040 (2009).
908 14. Suárez, L. E., Markello, R. D., Betzel, R. F. & Misic, B. Linking Structure and
909 Function in Macroscale Brain Networks. *Trends in Cognitive Sciences* **24**, 302–315
910 (2020).
911 15. Battiston, F. *et al.* The physics of higher-order interactions in complex systems. *Nat.*
912 *Phys.* **17**, 1093–1098 (2021).
913 16. Griffa, A., Amico, E., Liégeois, R., Ville, D. V. D. & Preti, M. G. Brain structure-
914 function coupling provides signatures for task decoding and individual fingerprinting.
915 *NeuroImage* 118970 (2022) doi:10.1016/j.neuroimage.2022.118970.
916 17. Gutierrez-Barragan, D. *et al.* Unique spatiotemporal fMRI dynamics in the awake
917 mouse brain. *Current Biology* **32**, 631-644.e6 (2022).
918 18. Preti, M. G. & Van De Ville, D. Decoupling of brain function from structure reveals
919 regional behavioral specialization in humans. *Nature Communications* **10**, 4747 (2019).
920 19. Baum, G. L. *et al.* Development of structure–function coupling in human brain
921 networks during youth. *PNAS* **117**, 771–778 (2020).
922 20. Buckner, R. L. & Krienen, F. M. The evolution of distributed association networks in
923 the human brain. *Trends in Cognitive Sciences* **17**, 648–665 (2013).
924 21. van den Heuvel, M. P., Bullmore, E. T. & Sporns, O. Comparative Connectomics.
925 *Trends in Cognitive Sciences* **20**, 345–361 (2016).
926 22. Assaf, Y., Bouznach, A., Zomet, O., Marom, A. & Yovel, Y. Conservation of brain
927 connectivity and wiring across the mammalian class. *Nat Neurosci* **23**, 805–808 (2020).
928 23. Avena-Koenigsberger, A. *et al.* Path ensembles and a tradeoff between
929 communication efficiency and resilience in the human connectome. *Brain Struct Funct*
930 **222**, 603–618 (2017).
931 24. Zhou, D. *et al.* Efficient coding in the economics of human brain connectomics.
932 *Network Neuroscience* 1–40 (2022) doi:10.1162/netn_a_00223.
933 25. Bettinardi, R. G. *et al.* How structure sculpts function: Unveiling the contribution of
934 anatomical connectivity to the brain's spontaneous correlation structure. *Chaos* **27**,

047409 (2017).

26. Goñi, J. *et al.* Exploring the Morphospace of Communication Efficiency in Complex Networks. *PLOS ONE* **8**, e58070 (2013).

27. Hao, Y. & Graham, D. Creative destruction: Sparse activity emerges on the mammal connectome under a simulated communication strategy with collisions and redundancy. *Network Neuroscience* **4**, 1055–1071 (2020).

28. Mišić, B. *et al.* Cooperative and Competitive Spreading Dynamics on the Human Connectome. *Neuron* **86**, 1518–1529 (2015).

29. Estrada, E. & Hatano, N. Communicability in complex networks. *Phys. Rev. E* **77**, 036111 (2008).

30. Friedrich, P. *et al.* Imaging evolution of the primate brain: the next frontier? *NeuroImage* **228**, 117685 (2021).

31. Ardesch, D. J. *et al.* Evolutionary expansion of connectivity between multimodal association areas in the human brain compared with chimpanzees. *PNAS* **116**, 7101–7106 (2019).

32. Xu, T. *et al.* Cross-species functional alignment reveals evolutionary hierarchy within the connectome. *NeuroImage* **223**, 117346 (2020).

33. Krubitzer, L. The Magnificent Compromise: Cortical Field Evolution in Mammals. *Neuron* **56**, 201–208 (2007).

34. Mesulam, M. M. From sensation to cognition. *Brain* **121**, 1013–1052 (1998).

35. Amico, E. *et al.* Toward an information theoretical description of communication in brain networks. *Network Neuroscience* 1–20 (2021) doi:10.1162/netn_a_00185.

36. Cover, T. M. & Thomas, J. A. ELEMENTS OF INFORMATION THEORY. 774 (2006).

37. Lambiotte, R., Rosvall, M. & Scholtes, I. From networks to optimal higher-order models of complex systems. *Nature Physics* **15**, 313–320 (2019).

38. Margulies, D. S. *et al.* Situating the default-mode network along a principal gradient of macroscale cortical organization. *PNAS* **113**, 12574–12579 (2016).

39. Amico, E. & Goñi, J. The quest for identifiability in human functional connectomes.

963 *Sci Rep* **8**, 1–14 (2018).

964 40. Finn, E. S. *et al.* Functional connectome fingerprinting: identifying individuals using
965 patterns of brain connectivity. *Nature Neuroscience* **18**, 1664–1671 (2015).

966 41. Messé, A. Parcellation influence on the connectivity-based structure–function
967 relationship in the human brain. *Human Brain Mapping* **41**, 1167–1180 (2020).

968 42. Birn, R. M. *et al.* The effect of scan length on the reliability of resting-state fMRI
969 connectivity estimates. *NeuroImage* **83**, 550–558 (2013).

970 43. Paquola, C. *et al.* Microstructural and functional gradients are increasingly
971 dissociated in transmodal cortices. *PLOS Biology* **17**, e3000284 (2019).

972 44. Bruner, E., Preuss, T. M., Chen, X. & Rilling, J. K. Evidence for expansion of the
973 precuneus in human evolution. *Brain Struct Funct* **222**, 1053–1060 (2017).

974 45. Xu, T. *et al.* Interindividual Variability of Functional Connectivity in Awake and
975 Anesthetized Rhesus Macaque Monkeys. *Biological Psychiatry: Cognitive Neuroscience*
976 *and Neuroimaging* **4**, 543–553 (2019).

977 46. Mueller, S. *et al.* Individual Variability in Functional Connectivity Architecture of the
978 Human Brain. *Neuron* **77**, 586–595 (2013).

979 47. Barttfeld, P. *et al.* Signature of consciousness in the dynamics of resting-state brain
980 activity. *Proceedings of the National Academy of Sciences* **112**, 887–892 (2015).

981 48. Luppi, A. I. *et al.* Consciousness-specific dynamic interactions of brain integration
982 and functional diversity. *Nature Communications* **10**, (2019).

983 49. Vézquez-Rodríguez, B., Liu, Z.-Q., Hagmann, P. & Misic, B. Signal propagation via
984 cortical hierarchies. *Network Neuroscience* **4**, 1072–1090 (2020).

985 50. Battiston, F. *et al.* Networks beyond pairwise interactions: Structure and dynamics.
986 *Physics Reports* **874**, 1–92 (2020).

987 51. Honey, C. J. *et al.* Slow Cortical Dynamics and the Accumulation of Information over
988 Long Timescales. *Neuron* **76**, 423–434 (2012).

989 52. Murray, J. D. *et al.* A hierarchy of intrinsic timescales across primate cortex. *Nat*
990 *Neurosci* **17**, 1661–1663 (2014).

991 53. Fries, P., Reynolds, J. H., Rorie, A. E. & Desimone, R. Modulation of Oscillatory
992 Neuronal Synchronization by Selective Visual Attention. *Science* **291**, 1560–1563 (2001).
993 54. Reimann, M. W. *et al.* Cliques of Neurons Bound into Cavities Provide a Missing Link
994 between Structure and Function. *Front. Comput. Neurosci.* **11**, (2017).
995 55. Van Essen, D. C. *et al.* The WU-Minn Human Connectome Project: An overview.
996 *NeuroImage* **80**, 62–79 (2013).
997 56. Glasser, M. F. *et al.* The minimal preprocessing pipelines for the Human
998 Connectome Project. *NeuroImage* **80**, 105–124 (2013).
999 57. Schaefer, A. *et al.* Local-Global Parcellation of the Human Cerebral Cortex from
1000 Intrinsic Functional Connectivity MRI. *Cereb Cortex* **28**, 3095–3114 (2018).
1001 58. Tournier, J.-D. *et al.* MRtrix3: A fast, flexible and open software framework for
1002 medical image processing and visualisation. *NeuroImage* **202**, 116137 (2019).
1003 59. Shen, K. *et al.* A macaque connectome for large-scale network simulations in
1004 TheVirtualBrain. *Sci Data* **6**, 123 (2019).
1005 60. Kötter, R. & Wanke, E. Mapping brains without coordinates. *Philosophical*
1006 *Transactions of the Royal Society B: Biological Sciences* **360**, 751–766 (2005).
1007 61. Baumann, S. *et al.* Orthogonal representation of sound dimensions in the primate
1008 midbrain. *Nat Neurosci* **14**, 423–425 (2011).
1009 62. Milham, M. P. *et al.* An Open Resource for Non-human Primate Imaging. *Neuron*
1010 **100**, 61-74.e2 (2018).
1011 63. Manjón, J. V., Coupé, P., Martí-Bonmatí, L., Collins, D. L. & Robles, M. Adaptive
1012 non-local means denoising of MR images with spatially varying noise levels. *Journal of*
1013 *Magnetic Resonance Imaging* **31**, 192–203 (2010).
1014 64. Smith, S. M. Fast robust automated brain extraction. *Human Brain Mapping* **17**, 143–
1015 155 (2002).
1016 65. Avants, B. B. *et al.* A reproducible evaluation of ANTs similarity metric performance
1017 in brain image registration. *NeuroImage* **54**, 2033–2044 (2011).
1018 66. Jenkinson, M., Bannister, P., Brady, M. & Smith, S. Improved Optimization for the

Robust and Accurate Linear Registration and Motion Correction of Brain Images. *NeuroImage* **17**, 825–841 (2002).

67. Mandino, F., Yeow Ling Yun, Gigg, J., Olivo, M. C. & Joanes Grandjean. Mouse_rest_3xTG. (2019) doi:10.18112/OPENNEURO.DS001890.V1.0.1.

68. Mandino, F., Yeow, L. Y., Gigg, J., Olivo, M. & Grandjean, J. Preserved functional networks in a hydrocephalic mouse. *Matters* **5**, e201905000001 (2019).

69. Grandjean, J., Schroeter, A., Batata, I. & Rudin, M. Optimization of anesthesia protocol for resting-state fMRI in mice based on differential effects of anesthetics on functional connectivity patterns. *NeuroImage* **102**, 838–847 (2014).

70. Oh, S. W. *et al.* A mesoscale connectome of the mouse brain. *Nature* **508**, 207–214 (2014).

71. Grandjean, J. *et al.* Chronic psychosocial stress in mice leads to changes in brain functional connectivity and metabolite levels comparable to human depression. *NeuroImage* **142**, 544–552 (2016).

72. Yeo, B. T. *et al.* The organization of the human cerebral cortex estimated by intrinsic functional connectivity. *J Neurophysiol* **106**, 1125–1165 (2011).

73. Kötter, R. *et al.* Advanced database methodology for the Collation of Connectivity data on the Macaque brain (CoCoMac). *Philosophical Transactions of the Royal Society of London. Series B: Biological Sciences* **356**, 1159–1186 (2001).

74. Kötter, R. Online retrieval, processing, and visualization of primate connectivity data from the CoCoMac Database. *Neuroinform* **2**, 127–144 (2004).

75. Stephan, K. E., Zilles, K. & Kötter, R. Coordinate–independent mapping of structural and functional data by objective relational transformation (ORT). *Philosophical Transactions of the Royal Society of London. Series B: Biological Sciences* **355**, 37–54 (2000).

76. Pijnenburg, R. *et al.* Myelo- and cytoarchitectonic microstructural and functional human cortical atlases reconstructed in common MRI space. *NeuroImage* **239**, 118274 (2021).

1047 77. Zerbi, V., Grandjean, J., Rudin, M. & Wenderoth, N. Mapping the mouse brain with
1048 rs-fMRI: An optimized pipeline for functional network identification. *NeuroImage* **123**, 11–
1049 21 (2015).
1050 78. Greicius, M. D., Krasnow, B., Reiss, A. L. & Menon, V. Functional connectivity in the
1051 resting brain: A network analysis of the default mode hypothesis. *PNAS* **100**, 253–258
1052 (2003).
1053 79. Vincent, J. L. *et al.* Intrinsic functional architecture in the anaesthetized monkey
1054 brain. *Nature* **447**, 83–86 (2007).
1055 80. Gozzi, A. & Schwarz, A. J. Large-scale functional connectivity networks in the rodent
1056 brain. *NeuroImage* **127**, 496–509 (2016).
1057 81. Grandjean, J. *et al.* Common functional networks in the mouse brain revealed by
1058 multi-centre resting-state fMRI analysis. *NeuroImage* **205**, 116278 (2020).
1059 82. Whitesell, J. D. *et al.* Regional, Layer, and Cell-Type-Specific Connectivity of the
1060 Mouse Default Mode Network. *Neuron* **109**, 545-559.e8 (2021).
1061 83. Timme, N. M. & Lapish, C. A Tutorial for Information Theory in Neuroscience. *eNeuro*
1062 **5**, (2018).
1063 84. Dimitrov, A. G., Lazar, A. A. & Victor, J. D. Information theory in neuroscience. *J*
1064 *Comput Neurosci* **30**, 1–5 (2011).
1065 85. Shannon, C. E. A Mathematical Theory of Communication. 53.
1066 86. Yen, J. Y. Finding the K Shortest Loopless Paths in a Network. *Management Science*
1067 **17**, 712–716 (1971).
1068